Journal of Materials Chemistry C

Accepted Manuscript

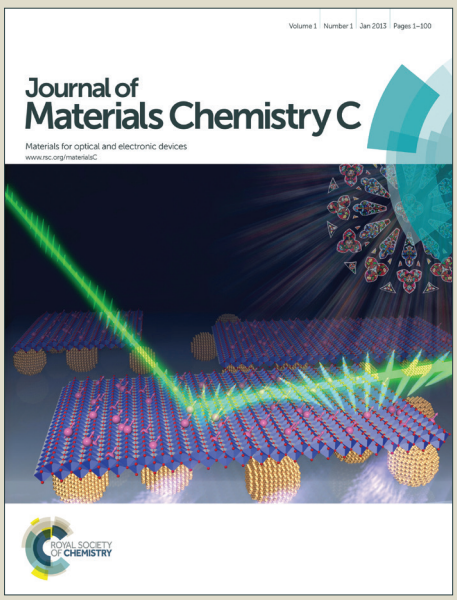

ROYAL SOCIETY OF CHEMISTRY

www.rsc.org/materialsC

Effect of Al/Si Substitution on the Structure and Luminescence Properties of $CaSrSiO_4:Ce^{3+}$ Phosphor: Analysis based on the Polyhedral Distortion†

Shihai Miao[1], Zhiguo Xia[1,2,*], Maxim S. Molokeev[3,4], Mingyue Chen[2], Jie Zhang[1], Quanlin Liu[2]

[1]*School of Materials Sciences and Technology, China University of Geosciences, Beijing 100083, China*

[2]*School of Materials Sciences and Engineering, University of Science and Technology Beijing, Beijing 100083, China*

[3]*Laboratory of Crystal Physics, Kirensky Institute of Physics, SB RAS, Krasnoyarsk 660036, Russia*

[4]*Department of Physics, Far Eastern State Transport University, Khabarovsk, 680021 Russia*

[*]Corresponding authors:

Zhiguo Xia E-mail: xiazg@ustb.edu.cn

School of Materials Sciences and Engineering, University of Science and Technology Beijing, Beijing 100083, China

Tel. : +86-10-8237-7955;

Fax. : +86-10-8237-7955

†Electronic supplementary information (ESI) available. The fractional atomic coordinates and isotropic displacement parameters ($Å^2$) and the corresponding crystallographic information files (CIF)of $(Ca_{0.95}Sr_{0.95}Ce_{0.05}Li_{0.05})(Si_{1-x}Al_x)O_4$ (x = 0, 0.01 and 0.1) were given.

ABSTRACT: Blue-emitting $CaSrSiO_4:Ce^{3+},Li^+$ phosphors were prepared by the high temperature solid-state method, and the effect of substitution of Al^{3+} for Si^{4+} in the $CaSrSiO_4:Ce^{3+},Li^+$ has been studied. Crystal structures of as-prepared $Ca_{1-y}Sr_{1-y}Si_{1-x}Al_xO_4:yCe^{3+},yLi^+$ were resolved by the Rietveld method, suggesting that all the samples belonged to orthorhombic symmetry (*Pnma*) of α-$CaSrSiO_4$. The photoluminescence (PL) emission and excitation spectra, lifetime, and the effect of Al^{3+} concentration on PL properties were investigated in detail. The emission peaks of $CaSrSi_{1-x}Al_xO_4:Ce^{3+},Li^+$ (x = 0 – 0.10) phosphors were red-shifted from 452 to 472 nm with increasing Al/Si ratio. The red-shift of the Ce^{3+} emission was ascribed to the polyhedra distortion of the cations originating from the variation of the neighboring $[(Si,Al)O_4]$ polyhedral, and the detailed mechanism has been discussed.

1. INTRODUCTION

Solid-state white lighting with superior efficiency, longer duration time, and tunable optical performance is in process of the replacement of traditional fluorescent and incandescent light sources. Among them, phosphor converted light emitting diodes (pc-LEDs) have been widely studied and applied as a fourth-generation light source.[1-4] Yellow-emitting phosphor $Y_3Al_5O_{12}:Ce^{3+}$ (YAG:Ce) by a combination of blue InGaN LED chip for *w*LEDs becomes the main stream. Except for the well-known YAG:Ce system, some other matrices can also act as the excellent phosphor hosts, such as nitrides/oxynitrides, silicates/borates or molybdates/tungstates, and so on, which show excellent photoluminescence (PL) properties.[5-8] The silicate phosphors represented by Eu^{2+} or Ce^{3+} doped orthosilicates A_2SiO_4 (A = Ca, Sr, Ba) have drew much attentions owing to their broad excitation/emission bands, tunable optical properties, moderate synthesis method and low fabrication cost.[9]

Based on a review for the recent papers on the main research topics and the important considerations in the design of new orthosilicates phosphors, there are three aspects needed to be developed in the future.[9-15] One is that the nitridation of the orthosilicates phosphors can induce red-shift of emission peaks. For example, Park reported the red-emitting phosphors $Sr_{2-y-z}Ca_zSi(O_{1-x}N_x)_4:yEu^{2+}$, and the nitridation effect led to a dramatic change in the crystal field.[11] Black found the new orange-red-emitting Eu^{2+}/Ce^{3+} doped $LaBaSiO_3N$ and $LaSrSiO_3N$ phosphors with β-K_2SiO_4 structure.[12] Another one is the design of the donor/acceptor couple in the A_2SiO_4 phase, and tunable emission can happen via the energy transfer of the codoped

ions, such as full-color emitting phosphor $Ba_{1.3}Ca_{0.7}SiO_4:Eu^{2+},Mn^{2+}$ and $Ba_{1.55}Ca_{0.45}SiO_4:Eu^{2+},Mn^{2+}$.[13,14] The last one is the exploration of the A_2SiO_4-based phosphors via the composition optimization and structural modification. Cheetham's group carefully investigated the phase relationship of Ca_2SiO_4 and found that suitable way to stabilize the γ-Ca_2SiO_4 phase and developed the yellow emitting phosphors for pc-LEDs.[3] Seshadri's group reported the $Sr_xBa_{2-x}SiO_4:Eu^{2+}$ phosphors, and the intermediate composition with 46% Sr has the optimum luminescence properties.[15]

As far as we know, luminescent properties of Ce^{3+} doped $CaSrSiO_4$ have not been reported. As also mentioned above, the intermediate compositions in the M_2SiO_4 phase brings us some opportunity to search for new phosphors. In this work, we studied the luminescent properties of blue-emitting $CaSrSiO_4:Ce^{3+},Li^+$ phosphors, and the effect of substitution of Al^{3+} with Si^{4+} in the $CaSrSiO_4:Ce^{3+},Li^+$ has been studied. Crystal structures and luminescence properties of $CaSrSi_{1-x}Al_xO_4:Ce^{3+},Li^+$ (x = 0 – 0.10) phosphors with increasing Al/Si ratio have been discussed, and observed red-shift was ascribed to the polyhedra distortion of cations occupied by Ce^{3+}.

2. EXPERIMENTAL

The designed $Ca_{1-y}Sr_{1-y}Si_{1-x}Al_xO_4:yCe^{3+},yLi^+$ phosphors were synthesized by conventional high temperature solid-state reaction. The starting materials were as follows, $SrCO_3$ (A.R.), $CaCO_3$ (A.R.), Li_2CO_3 (A.R.), SiO_2 (A.R.), Al_2O_3 (A.R.) and CeO_2 (99.99%). After mixing and grinding in an agate mortar for 25 min, the mixture was placed in a crucible and then sintered at 1400 °C for 5 h in a reducing atmosphere

of H_2 (10%) and N_2 (90%) to produce the final samples. Finally, the prepared phosphors were cooled to room temperature and reground for further measurements.

The powder X-ray diffraction (XRD) measurements were performed on D8 Advance diffractometer (Bruker Corporation, Germany) operating at 40 kV and 40 mA with Cu Kα radiation (λ = 1.5406 Å). The scanning rate for phase identification was fixed at 4°/min with 2θ ranges from 10° to 70° and the data for Rietveld analysis were collected in a step-scanning mode with the step size of 0.02° and 10 s counting time per step over the 2θ range from 10° to 120°. The PL and photoluminescence excitation (PLE) spectra were recorded by a Hitachi F–4600 spectrophotometer equipped with a 150 W xenon lamp as the excitation source. The decay curves were recorded on an Edinburgh instrument (FLSP920) with a nF900 flash lamp was used as the excitation resource. Quantum efficiency was measured using the integrating sphere on the same FLSP920 fluorescence spectrophotometer.

3. RESULTS AND DISCUSSION

XRD patterns of all the as-prepared $Ca_{0.95}Sr_{0.95}Si_{1-x}Al_xO_4$:0.05$Ce^{3+}$,0.05$Li^+$ (x = 0, 0.1, 0.2, 0.3, 0.4, 0.5, 0.7 and 0.8) phosphors were given in Fig.1a. Although the designed chemical formula didn't fulfil the charge balance seemingly, this may be overcome with some vacancies (point defects) in the oxygen lattice. The standard data for $CaSrSiO_4$ (JCPDS 72-2260) is also shown as a reference in Fig.1a. The magnified XRD patterns between 31° and 34° were demonstrated in Fig.1b. From the compared results on the variation of the diffraction peaks in Fig.1, we can see that the obtained

samples can be basically indexed to the $CaSrSiO_4$ phase (JCPDS 72-2260) when $x \leq 0.1$. Some diffraction peaks ascribed to the impurity appear in the vicinity of 33° when the doping amount of Al^{3+} is more than $x = 0.1$, therefore the maximum dissolution amount of Al substituted Si in $CaSrSiO_4$ host should be below $x = 0.1$.

In order to further investigate the phase formation depending on the Al/Si substitution of $Ca_{0.95}Sr_{0.95}Si_{1-x}Al_xO_4$:$0.05Ce^{3+}$,$0.05Li^+$ phosphors, XRD patterns for the selected samples with different Al/Si substitution amount of $x = 0.01$ and $x = 0.1$ for $Ca_{0.95}Sr_{0.95}SiO_4$:$0.05Ce^{3+}$,$0.05Li^+$ were shown in Fig.2a. The three samples shown in Fig.2a clearly indicated that all the diffraction peaks of the selected samples agree well with the standard data for the orthorhombic phase of $CaSrSiO_4$ (JCPDS 72-2260), suggesting that they belong to the pure phase as mentioned in Fig.1. Accordingly, the powder diffraction data of $(Ca_{0.95}Sr_{0.95}Ce_{0.05}Li_{0.05})(Si_{1-x}Al_x)O_4$ ($x = 0$, 0.01 and 0.1) were then refined via the Rietveld analysis performed by using TOPAS 4.2. The Rietveld plots for three samples were shown in Fig.2b, Fig.2c and Fig.2d, respectively, and the main parameters of processing and refinement were listed in Table 1. As shown in Fig. 2b-d, almost all peaks were indexed by orthorhombic cell (*Pnma*) with parameters close to α-$CaSrSiO_4$. Therefore crystal structure of $CaSrSiO_4$ was taken as starting model for Rietveld refinement. Fig.3 demonstrated the representative crystal structure of $(Ca_{0.95}Sr_{0.95}Ce_{0.05}Li_{0.05})(Si_{1-x}Al_x)O_4$ and the coordination environment of Ca1/Sr1 and Ca2/Sr2 ions doped by Ce^{3+} and Li^+. As far as we know, there are two Ca/Sr sites in $CaSrSiO_4$ structure with different coordination numbers, 10-coordinated Ca1/Sr1 site and 9-coordinated Ca2/Sr2 site,

and each of them is disordered by Ca/Sr with occupancy 1/2. The same model was realized in our model for the study of $(Ca_{0.95}Sr_{0.95}Ce_{0.05}Li_{0.05})(Si_{1-x}Al_x)O_4$, and Ca/Sr occupations were also refined, but sum of their occupations were equal to 0.475 instead of 0.5 because Ce^{3+} and Li^+ ions also existed in this sites with occupancies 0.0125 and 0.0125 respectively. Based on the above crystal structure analysis, refinement in such a model was stable and gives low R-factors (Table 1, Fig.2b-2d) suggesting that phase structures keep invariable with the introduction of Al. Cell volume of compound with $x = 0.1$ is bigger than cell volume of $x = 0.01$ and $x = 0$, which is in accordance with bigger value of ion radii (IR) of Al^{3+} (CN = 4, IR = 0.39 Å) in comparison with IR of Si^{4+} (CN = 4, IR = 0.26 Å).[16] The fractional atomic coordinates and isotropic displacement parameters ($Å^2$) of $(Ca_{0.95}Sr_{0.95}Ce_{0.05}Li_{0.05})(Si_{1-x}Al_x)O_4$ ($x = 0$, 0.01 and 0.1) were given in Table S1, and the corresponding crystallographic information files (CIF) for them were also presented in electronic supplementary information (ESI).

The PL and PLE spectra of $Ca_{0.95}Sr_{0.95}SiO_4$:0.05Ce^{3+},0.05Li^+ were shown in Fig.4a. The PLE spectrum monitored at 452nm exhibits a broad band from 200 to 450 nm, indicating a complex splitting of the $5d^1$ excited state of Ce^{3+}. The emission spectrum showed a broad band peaking at 452 nm when excited at 365nm. Based on the Gaussian fitting, the PL spectrum in Fig.4a could be divided into two Gaussian peaks at 440 nm (22727 cm^{-1}) and 475 nm (21053 cm^{-1}), and the energy difference was calculated to be 1673 cm^{-1}, which showed difference compared with the theoretical value of 2000 cm^{-1} for the $^2F_{7/2}$ and $^2F_{5/2}$ states of Ce^{3+}. Therefore we

proposed that Ce/Li are located as two kinds of Ca/Sr sites and eventually two kinds of luminescent centers are formed. Moreover, the emission positions of the Ce^{3+} ion is strongly dependent on its local environment, which has been suggested to obey an empirical relation between the energetic position of the Ce^{3+} emission and the local structure in various compounds. The equation is given as follows[17],

$$E = Q\left[1-\left(\frac{V}{4}\right)^{\frac{1}{V}}10^{-\frac{n\times Ea\times r}{80}}\right] \quad (1)$$

Herein, E represents the real position of the d-band edge in energy for Ce^{3+} (cm^{-1}), Q is the position in energy for the lower d-band edge for the Ce^{3+} free ions, V is the valence of the Ce^{3+} ion, n is the number of anions in the immediate shell about this ion, and r is the radius of the host cation replaced by the Ce^{3+} ion (Å). Ea is the electron affinity of the atoms that form anions. In the present case, there are two Ca/Sr sites in $CaSrSiO_4$ structure. Therefore, most parameters keep invariable in the Eq.(1), so that the coordination number n is proportional to the observed position of the d-band edge for Ce^{3+}. As a result, Ce^{3+} center showing emission peak at 440 nm occupied the 10-coordinated Ca^{2+}/Sr^{2+} site, and the other Ce^{3+} center showing 475 nm was related with the 9-coordinated Ca^{2+}/Sr^{2+} site.

The influence of the polyhedron on the crystal field splitting can be denoted by ε_{cfs} value.[18-19] A large ε_{cfs} value is the main reason for the great red shift of the first f–d transition, and there is an empirical relationship between ε_{cfs} value and the average distance (R) between the activator and the neighboring anions,

$$\varepsilon_{cfs} = \beta_{poly}^{Q} R_{av}^{-2} \quad (2)$$

where R_{av} is close to the average distance between anions and cations that is replaced

by Ce^{3+}, β_{poly} is a constant that depends on the type of the coordinating polyhedron and Q is 3 for Ce^{3+}. β_{poly} values are in the ratio 1, 0.89, 0.79, 0.42 for octahedral, cubic, dodecahedral, and tricapped trigonal prismatic coordination, respectively. ε_{cfs} is likely to decrease with the increase in coordination number and the average distance (R).

Except for the crystal field splitting, centroid shift also influences the energy of the lowest excited 5d level. The 5d centroid shift for Ce^{3+} can be expressed by the following equation:

$$\varepsilon_c = A\sum_{i=1}^{N}\frac{\alpha_{SP}^{i}}{(R_i - 0.6\Delta R)^6} \qquad (3)$$

where R_i is the distance (pm) between Ce^{3+} and anion i in the undistorted lattice. The summation is over all O anions that coordinate Ce^{3+}. $0.6\Delta R$ is a correction for lattice relaxation around Ce^{3+}, and ΔR is the difference between the radii of Ce^{3+} and Ca^{2+}/Sr^{2+} in different sites. $\alpha_{sp}^{i}(10^{-30}m^{-3})$ is the spectroscopic polarizability of anion i. A is a constant as 1.79×10^{13}. The values of ε_c for Ce^{3+} on Ca1/Sr1(ten-coordinate) is smaller than Ce^{3+}on Ca2/Sr2(nine-coordinate), by introducing the values of N, R_i and ΔR.[18-19]

Fig.4b gave the PL spectra of $Ca_{1-x}Sr_{1-x}SiO_4{:}xCe^{3+},xLi^{+}$ (x = 0.01, 0.03, 0.05, 0.08, 0.10, 0.15 and 0.20). Owing to the 5*d*-4*f* allowed transition of Ce^{3+}, the emission spectra consist of an asymmetric broad band centered at 452 nm. The emission intensities have a increasing trend with increasing Ce^{3+} concentration, and maximize at x = 0.05, and then decrease, which could be attributed to the internal concentration quenching effect. Also from the PL intensities as a function of Ce^{3+} content in Fig.4c we can conclude that the quenching concentration of Ce^{3+} appears at x = 0.05. As we

know, non-radiative energy transfer between different Ce^{3+} ions may occur by exchange interaction, radiation reabsorption, or multipole–multipole interaction. The critical energy transfer distance between Ce^{3+} ions can be calculated by using concentration quench equation (4) proposed by Blasse:[20]

$$R_c \approx 2\left(\frac{3V}{4\pi x_c N}\right)^{\frac{1}{3}} \quad (4)$$

where V is the volume of unit cell, x_c is the critical concentration, N is the number of cations in the unit cell and V is the volume of the unit cell. Herein, $V = 366.95$ Å^3, $N = 8$ and x_c is 0.05 in the $Ca_{1-x}Sr_{1-x}SiO_4$:xCe^{3+},xLi^+. According to the above equation, the critical distance of energy transfer is estimated to be about 12.05 Å. Therefore, according to the Dexter theory, the non-radiative transitions between Eu^{2+} ions took place via electric multipolar interactions.[21] The interaction type between sensitizers or between sensitizer and activator can be calculated by the following equation (5): [22-23]

$$\frac{I}{x} = K\left[1+\beta(x)^{\theta/3}\right]^{-1} \quad (5)$$

where I is the emission intensity, x is the concentration of the activator ions beyond the critical concentration of $x = 0.05$, β and K are constant under the same excitation condition, and θ is an indication of electric multipolar character. Based on the previous report, $\theta = 3$ for the energy transfer among the nearest-neighbor ions, while $\theta = 6$, 8 and 10 for dipole–dipole (d–d), dipole–quadrupole (d–q), and quadrupole–quadrupole (q–q) interactions, respectively. In order to obtain a correct value of θ for the emission centers, the dependence of $\lg(I/x)$ on $\lg(x)$ is presented, and it yield a straight line with a slope equal to -θ/3. The fitting plot for Ce^{3+} emission

centers corresponding to the concentrations above Ce^{3+} quenching concentration is shown in Fig.4d. The slope is -1.711, and the value of θ can be calculated as 5.133, which is more closely to 6. This result verified that the concentration quenching in $Ca_{1-x}Sr_{1-x}SiO_4:xCe^{3+},xLi^+$ phosphor is ascribed to the dipole–dipole interaction.[24]

As reported previously, the addition of Al in the Ca_2SiO_4 host can stabilize the γ-Ca_2SiO_4 phase and further change the emission colors of Ce^{3+} in the studied host owing to the formation of new polymorphs.[3] The PLE and PL spectra of $Ca_{0.95}Sr_{0.95}Si_{0.9}Al_{0.1}O_4:0.05Ce^{3+},0.05Li^+$ were given in Fig.5a. In the excitation spectrum, it is similar as that of $Ca_{0.95}Sr_{0.95}SiO_4:0.05Ce^{3+},0.05Li^+$ with a broad band. Under 365 nm UV light excitation, $Ca_{0.95}Sr_{0.95}Si_{0.9}Al_{0.1}O_4:0.05Ce^{3+},0.05Li^+$ phosphor showed an emission band ranging from 400 to 600 nm with a maximum at 472 nm. Comparing with the emission spectrum of $Ca_{0.95}Sr_{0.95}SiO_4:0.05Ce^{3+},0.05Li^+$ phosphor, we can find an apparent red shift owing to the Al/Si substitution even if the phase structure keeps invariable as discussed above. Therefore, the effect of Al/Si substitution on the luminescence properties of $Ca_{0.95}Sr_{0.95}SiO_4:0.05Ce^{3+},0.05Li^+$ phosphors has been studied, and the doped Ce^{3+} concentration is fixed at 0.05. The as-measured and normalized emission spectra for $Ca_{0.95}Sr_{0.95}Si_{1-x}Al_xO_4:0.05Ce^{3+},0.05Li^+$ (x = 0, 0.01, 0.03, 0.05, 0.08 and 0.10) phosphors under UV excitation (λ_{ex} = 365nm) were shown in Fig.5b and Fig.5c, respectively. As shown in Fig.5b, the emission intensities decrease sharply with the introduction of Al, however, it keeps nearly invariable in the range of x = 0.01-0.1. From Fig.5c we can see that the emission spectra gradually shift to the long

wavelength direction from 452 nm to 472 nm (red shift) with increasing Al/Si ratios. Except for the variation of the spectral profile, we have measured the internal quantum efficiency (QE) of the selected $Ca_{0.95}Sr_{0.95}Si_{1-y}Al_yO_4:0.05Ce^{3+},0.05Li^+$ (y = 0, 0.01, 0.1) phosphors. The measured QE of $Ca_{0.95}Sr_{0.95}Si_{1-y}Al_yO_4:0.05Ce^{3+},0.05Li^+$ (y = 0, 0.01, 0.1) phosphors are determined as 10.0% 39.2% 53.1%, respectively. It is believed that the QE can be further improved through optimization of the processing conditions in the future.

To study the dynamics of luminescence, we have measured the PL decay curves of Ce^{3+} in $Ca_{0.95}Sr_{0.95}Si_{1-x}Al_xO_4:0.05Ce^{3+},0.05Li^+$ phosphors. As depicted in Fig.5d, one can see the decay curves of Ce^{3+} emission in $Ca_{0.95}Sr_{0.95}Si_{1-x}Al_xO_4:0.05Ce^{3+},0.05Li^+$ phosphors all obey a second-order exponential decay, which can be fitted in this formula as follows: [25-26]

$$I(t) = I_0 + A_1 \exp(-t/\tau_1) + A_2 \exp(-t/\tau_2) \quad (6)$$

where t is the time, τ_1 and τ_2 are rapid and slow times for the exponential components, A_2 and A_1 are constants, and $I(t)$ is the luminescence intensity at time t. Then we can give the average lifetime τ^* by using the following Eq. (7)

$$\tau^* = (A_1\tau_1^2 + A_2\tau_2^2)/(A_1\tau_1 + A_2\tau_2) \quad (7)$$

The calculated average decay lifetimes of Ce^{3+} ions for $Ca_{0.95}Sr_{0.95}Si_{1-x}Al_xO_4:0.05Ce^{3+},0.05Li^+$ phosphors (x = 0, 0.01, 0.05, 0.10) are determined to be 39.9, 40.2, 41.4, and 42.5ns, respectively. We can see that the lifetime values have a slightly increase, but on the whole there is no obvious change.[27-28]

Although the phase structures of $Ca_{0.95}Sr_{0.95}Si_{1-x}Al_xO_4$:0.05$Ce^{3+}$,0.05$Li^+$ keep invariable depending on the Al/Si substitution, the emission peaks are red shifted suggesting that the local structures changed. Since the dopant Ce^{3+} will occupy the cations' site of Ca/Sr, crystal structure of investigated compounds consist of disordered $(Si,Al)O_4$ tetrahedra and two types of cations' polyhedra: $(Ca1/Sr1/Ce1/Li1)O_{10}$ and $(Ca2/Sr2/Ce2/Li2)O_9$, as also shown in Fig.3. Distortion of $(Ca1/Sr1/Ce1/Li1)O_{10}$ and $(Ca2/Sr2/Ce2/Li2)O_9$ polyhedra is linked with increasing average Al/Si ion size with increasing *x*. Calculation proves that average bond length (Al/Si–O) increases from 1.625 to 1.626 Å and 1.643 Å with increasing *x* from 0, to 0.01 and 0.1. Since $(Ca1/Sr1/Ce1/Li1)O_{10}$ and $(Ca2/Sr2/Ce2/Li2)O_9$ polyhedra connect with some $(Al/Si)O_4$ tetrahedra by edges and faces, increasing of $(Al/Si)O_4$ size leads to increasing some angles O–(Ca/Sr/Ce/Li)–O and of course distort polyhedra. The $(Al/Si)O_4$ tetrahedra which connect with polyhedra only by nodes also distort them due to d(Al/Si–O) enlarge but d(Ca/Sr/Ce/Li–O) shorten. Therefore, Fig.6 shows the schematic diagram of polyhedra distortion for $(Ca1/Sr1/Ce1/Li1)O_{10}$ and $(Ca2/Sr2/Ce2/Li2)O_9$ with increasing $(Al/Si)O_4$ tetrahedra size. The arrows show structure changes with increasing Al concentration, *x*. Herein, angles of O–(Ca/Sr/Ce/Li)–O marked by orange sectors increase with increasing *x*.

The average bond length $d(Ca1/Sr1–O)_{x=0}$=2.73(3) Å, $d(Ca1/Sr1–O)_{x=0.01}$=2.73(3) Å and $d(Ca1/Sr1–O)_{x=0.1}$=2.76(3) Å are bigger than $d(Ca2/Sr2–O)_{x=0}$=2.54(3) Å, $d(Ca2/Sr2–O)_{x=0.01}$=2.54(3) Å and $d(Ca2/Sr2–O)_{x=0.1}$=2.53(3) Å for compounds with $x = 0$, $x = 0.01$ and $x = 0.1$, respectively. The bigger coordination number of Ca1/Sr1

site in comparison with Ca2/Sr2 should be the reason for this. This fact proves that Sr ion more likely locates in Ca1/Sr1 site. As a result, the increasing values of x from 0 to 0.1 didn't lead to drastically change of Ca1/Sr1 or Ca2/Sr2 concentration and average bond lengths. Then, polyhedra distortion can be calculated by using the following formula: [29]

$$D = \frac{1}{n}\sum_{i=1}^{n}\frac{l_i - l_{av}}{l_{av}} \qquad (8)$$

where l_i is the distance from the central atom to the i^{th} coordinating atom, l_{av} is the average bond length. The calculated results showed that the value of $D(Ca1/Sr1)_{x=0.1}$=0.076 is bigger than that of $D(Ca1/Sr1)_{x=0.01}$=0.075 and that of $D(Ca1/Sr1)_{x=0}$=0.074 for the samples with x = 0.1, x = 0.01 and x = 0, respectively. Value of $D(Ca2/Sr2)_{x=0}$ = 0.033 for x = 0 also increases up to $D(Ca2/Sr2)_{x=0.01}$ = 0.041 and $D(Ca2/Sr2)_{x=0.1}$ = 0.048 for compounds with x = 0.01 and x = 0.1, respectively. Herein, we can draw a conclusion that the increasing of distortion of $(Ca1/Sr1/Ce1/Li1)O_{10}$ and $(Ca2/Sr2/Ce2/Li2)O_9$ polyhedra with increasing x can be the reason of red shift in these compounds.[30]

4. CONCLUSIONS

The effects of Al/Si substitution on the phase structures and luminescence properties of $CaSrSi_{1-x}Al_xO_4:Ce^{3+},Li^+$ phosphors were investigated in detail. The crystal structures keep invariable when the doping amount of Al is below x = 0.1. PL spectra show that when the values x increase from 0 to 0.1, the emission spectra are gradually red shifted. Crystal structure of $CaSrSi_{1-x}Al_xO_4:Ce^{3+},Li^+$ phosphors consist

of disordered $(Si,Al)O_4$ tetrahedra and two types of cations' polyhedra: $(Ca1/Sr1/Ce1/Li1)O_{10}$ and $(Ca2/Sr2/Ce2/Li2)O_9$. The increasing of distortion of $(Ca1/Sr1/Ce1/Li1)O_{10}$ and $(Ca2/Sr2/Ce2/Li2)O_9$ polyhedra with increasing x can be the reason of red shift. This result provides an impetus for the search for new phosphor hosts and explains the mechanism causes the red shift.

ACKNOWLEDGEMENTS

The present work was supported by the National Natural Science Foundations of China (Grant No. No.51002146, No.51272242), Natural Science Foundations of Beijing (2132050), the Program for New Century Excellent Talents in the University of the Ministry of Education of China (NCET-12-0950), Beijing Nova Program (Z131103000413047), Beijing Youth Excellent Talent Program (YETP0635), the Funds of the State Key Laboratory of New Ceramics and Fine Processing, Tsinghua University (KF201306) and Fundamental Research Funds for the Central Universities (FRF-TP-14-005A1).

REFERENCES

(1) S . Nakamura, M. Senoh and T. Mukai, *Appl. Phys. Lett.*, 1993, **62,** 2390-2392.

(2) Z. G. Xia, Y. Y. Zhang, M. Molokeev, V. V. Atuchin and Y. Luo, *Sci. Rep.*, 2013, **3**, 3310.

(3) A. Kalaji, M. Mikami and A. K. Cheetham, *Chem. Mater*., 2014, **26**, 3966-3975.

(4) F. W. Kang, Y. Zhang, L. Wondraczek, J. Q. Zhu, X. B. Yang and M. Y. Peng, *J. Mater. Chem. C*, 2014, **2**, 9850-9857.

(5) Z. Y. Hou, C. X. Li, J. Yang, H. Z. Lian, P. P. Yang, R. Chai, Z. Y. Cheng and J. Lin, *J. Mater. Chem*., 2009, **19**, 2737-2746.

(6) F. W. Kang and M. Y. Peng, *Dalton Trans.*, 2014, **43**, 277-284.

(7) Y. Y. Li, Q, S. Wu, X. C. Wang, J. Y. Ding, Q. Long and Y. H. Wang, *RSC. Adv*., 2014, **4**, 63569-63575.

(8) Y. Chen, Y. Li, J. Wang, M. M. Wu and C. X. Wang. *J. Phys. Chem. C*, 2014, **118**, 12494-12499.

(9) Z. D. Hao, J. H. Zhang, X. Zhang, Y. S. Luo, L. G. Zhang and H. F. Zhao, *J. Lumin*., 2014, **152**, 40-43.

(10) L. C. Ju, X. Xu, L. Y. Hao, Y. Lin and M. H. Lee, *J. Mater. Chem. C*, 2015, 3, 1567-1575.

(11) J. Park, S. J. Lee and Y. J. Kim, *Cryst. Growth Des*., 2013, **13**, 5204-5210.

(12) A. P. Black, K. A. Denault, J. Ora-Sole, A. R. Goni and A. Fuertes, *Chem. Commum*., 2015, **51**, 2166-2169

(13) W. Z. Lv, M. M. Jiao, Q. Zhao, B. Q. Shao, W. Lv and H. P. You, *Inorg. Chem*.,

2014, **53**, 11007-11014.

(14) S. H. Miao, Z. G. Xia, J. Zhang and Q. L. Liu, *Inorg. Chem.*, 2014, **53**, 10386-10393.

(15) K. A. Denault, J. Brgoch, M. W. Gaultois, A. Mikhailovsky, R. Petry, H. Winkler, S. P. DenBaars and R. Seshadri, *Chem. Mater*., 2014, **26**, 2275-2282.

(16) M. Catti, G. Gazzoni and G. Ivaldi, *Acta Cryst B*, 1984, **40**, 537-544.

(17) L. G. Van Uitert, *J. Lumin.*, 1984, **29**, 1.

(18) J. L. Zhang, W. L. Zhang, Y. A. He, W. L. Zhou, L. P. Yu, S. X. Lian, Z. Q. Li and M. L. Gong, *Ceram. Int*., 2014, **40**, 9831-9834.

(19) Y. A. He, J. L. Zhang, W. L. Zhou, J. Han, Z. X. Qiu, L. P. Yu, C. Y. Rong and S. X. Lian, *J. Am. Ceram. Soc*., 2014, **97**, 1517-1522.

(20) G. Blasse, *Philips Res. Rep.*, 1969, **24**, 131-144.

(21) H. H. Lin, G. B. Zhang, P. A. Tanner and H. B. Liang, *J. Phys. Chem. C*, 2013, **117**, 12769-12777.

(22) L. L. Zhang, J. H. Zhang, X. Zhang, Z. D. Hao, H. F. Zhao and Y. S. Luo, *ACS Appl. Mater. Interfaces*, 2013, **5**, 12839-12846.

(23) L. G. Van Uitert, *J. Electrochem. Soc*., 1967, **114**, 1048.

(24) R. J. Xie and N. Hirosaki, *Appl. Phys. Lett.*, 2007, **90**, 191101.

(25) G. G. Li, Y. Zhang, D. L. Geng, M. M. Shang, C. Peng, Z. Y. Cheng and J. Lin, *ACS Appl. Mater. Interfaces*, 2012, **4**, 296-305.

(26) T. Chengaiah, C. K. Jayasankar and L. R. Moorthy, *Physica. B*, 2013, **431**, 137-141.

(27) Z. G. Xia and W. W. Wu, *Dalton. Trans*., 2013, **42**, 12989-12997.

(28) Z. G. Xia and R. S. Liu, *J. Phys. Chem. C,* 2012, **116**, 15604.

(29) K. A. Denault, N. C. George, S. R. Paden, S. Brinkley, A. A. Mikhailovsky, J. Neuefeind, S. P. DenBaars and R. Seshadri, *J. Mater. Chem*., 2012, **22**, 18204-18213.

(30) W. H. Baur, *Acta Cryst B*, 1974, **30**, 1195-1215.

Table 1 Main parameters of processing and refinement of the $(Ca_{0.95}Sr_{0.95}Ce_{0.05}Li_{0.05})(Si_{1-x}Al_x)O_4$ (x = 0, 0.01 and 0.1) samples.

Compound	x=0	x=0.01	x=0.1
Sp.Gr.	*Pnma*	*Pnma*	*Pnma*
a, Å	6.9541(4)	6.9527(3)	6.9490(3)
b, Å	5.5826(3)	5.5872(3)	5.5922(3)
c, Å	9.4520(5)	9.4552(5)	9.4653(4)
V, Å^3	366.95(3)	367.30(3)	367.83(3)
Z	8	8	8
2θ-interval, º	5-120	5-120	5-120
No. reflections	309	309	309
No. refinement parameters	44	44	44
R_{wp}, %	14.24	12.59	11.54
R_p, %	10.27	9.52	8.80
R_{exp}, %	9.72	9.41	9.54
χ^2	1.46	1.34	1.21
R_B, %	4.66	3.44	2.73

FIGURE CAPTIONS

Figure 1 XRD patterns (a) and magnified patterns between 31° and 34° (b) of $Ca_{0.95}Sr_{0.95}Si_{1-x}Al_xO_4:0.05Ce^{3+},0.05Li^+$. The standard data for $CaSrSiO_4$ (JCPDS 72-2260) is shown as a reference.

Figure 2 (a) XRD patterns of $Ca_{0.95}Sr_{0.95}SiO_4:0.05Ce^{3+},0.05Li^+$ (i), $Ca_{0.95}Sr_{0.95}Si_{0.99}Al_{0.01}O_4:0.05Ce^{3+},0.05Li^+$ (ii), $Ca_{0.95}Sr_{0.95}Si_{0.9}Al_{0.1}O_4:0.05Ce^{3+},0.05Li^+$ (iii). The standard data for $CaSrSiO_4$ (JCPDS 72-2260) is shown as a reference. (b) Difference Rietveld plot of $(Ca_{0.95}Sr_{0.95}Ce_{0.05}Li_{0.05})(Si_{1-x}Al_x)O_4$, $x = 0$. (c) Difference Rietveld plot of $(Ca_{0.95}Sr_{0.95}Ce_{0.05}Li_{0.05})(Si_{1-x}Al_x)O_4$, $x = 0.01$. (d) Difference Rietveld plot of $(Ca_{0.95}Sr_{0.95}Ce_{0.05}Li_{0.05})(Si_{1-x}Al_x)O_4$, $x=0.1$.

Figure 3 (a) Crystal structure of $(Ca_{0.95}Sr_{0.95}Ce_{0.05}Li_{0.05})(Si_{1-x}Al_x)O_4$; (b) coordination of Ca1/Sr1 and Ca2/Sr2 ions doped by Ce^{3+} and Li^+.

Figure 4 (a) PLE and PL spectra of $Ca_{0.95}Sr_{0.95}SiO_4:0.05Ce^{3+},0.05Li^+$ and the Gaussian fitting of the PL spectrum, (b) PL spectra of $Ca_{1-x}Sr_{1-x}SiO_4:xCe^{3+},xLi^+$ (x = 0.01, 0.03, 0.05, 0.08 and 0.10). (c) The PL intensity of the plot of $Ca_{1-2x}SrSiO_4:xCe^{3+},xLi^+$ as a function of Ce^{3+} content. (d) The relationships of lg(x) versus lg(I/x).

Figure 5 (a) PLE and PL spectra of $Ca_{0.95}Sr_{0.95}Si_{0.9}Al_{0.1}O_4:0.05Ce^{3+},0.05Li^+$, (b) PL spectra of $Ca_{0.95}Sr_{0.95}Si_{1-x}Al_xO_4:xCe^{3+},xLi^+$ (x = 0, 0.01, 0.03, 0.05, 0.08 and 0.10), (c) the normalized PL spectra. (d) Decay curves of Ce^{3+} emission in $Ca_{0.95}Sr_{0.95}Si_{1-x}Al_xO_4:0.05Ce^{3+},0.05Li^+$ phosphors under excitation at 365 nm, monitored at 452 nm.

Figure 6 Mechanism of distortion polyhedra: (a) $(Ca1/Sr1/Ce1/Li1)O_{10}$; (b) $(Ca2/Sr2/Ce2/Li2)O_9$ with increasing of $(Al/Si)O_4$ tetrahedra size. Blue arrows show structure changes with increasing Al concentration, *x*. Angles O–(Ca/Sr/Ce/Li)–O, which increase their values with *x*, are marked by orange sectors.

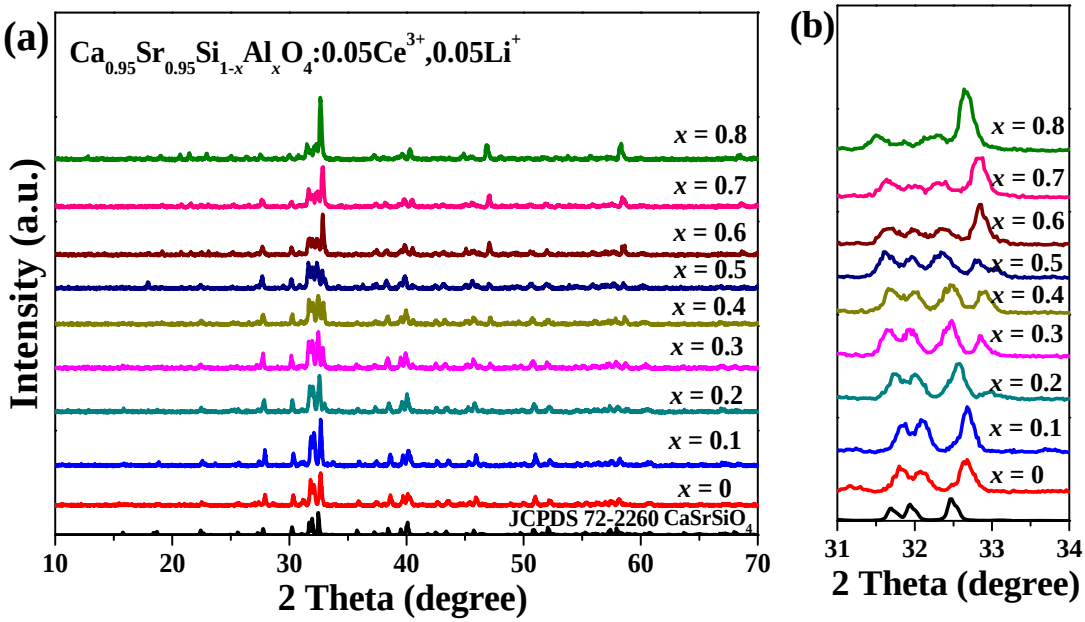

Figure 1 XRD patterns (a) and magnified patterns between 31° and 34° (b) of $Ca_{0.95}Sr_{0.95}Si_{1-x}Al_xO_4$:0.05$Ce^{3+}$,0.05$Li^+$. The standard data for $CaSrSiO_4$ (JCPDS 72-2260) is shown as a reference.

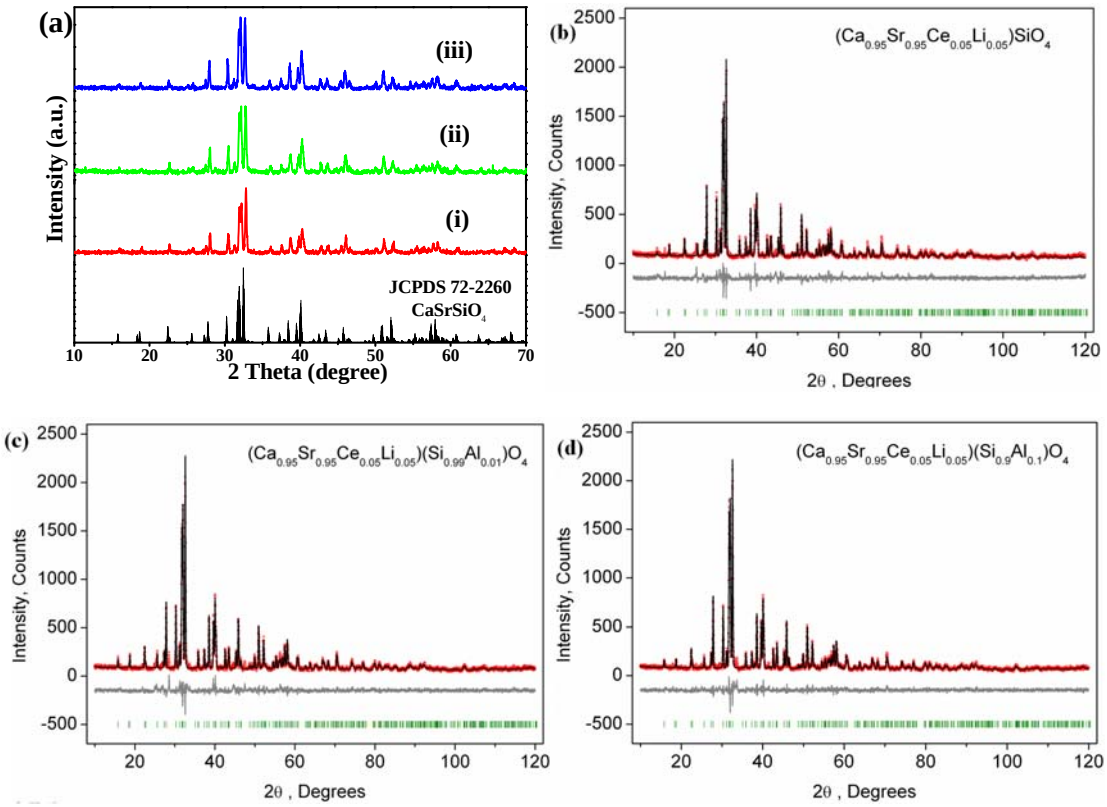

Figure 2 (a) XRD patterns of $Ca_{0.95}Sr_{0.95}SiO_4:0.05Ce^{3+},0.05Li^+$ (i), $Ca_{0.95}Sr_{0.95}Si_{0.99}Al_{0.01}O_4:0.05Ce^{3+},0.05Li^+$ (ii), $Ca_{0.95}Sr_{0.95}Si_{0.9}Al_{0.1}O_4:0.05Ce^{3+},0.05Li^+$ (iii). The standard data for $CaSrSiO_4$ (JCPDS 72-2260) is shown as a reference. (b) Difference Rietveld plot of $(Ca_{0.95}Sr_{0.95}Ce_{0.05}Li_{0.05})(Si_{1-x}Al_x)O_4$, $x = 0$. (c) Difference Rietveld plot of $(Ca_{0.95}Sr_{0.95}Ce_{0.05}Li_{0.05})(Si_{1-x}Al_x)O_4$, $x = 0.01$. (d) Difference Rietveld plot of $(Ca_{0.95}Sr_{0.95}Ce_{0.05}Li_{0.05})(Si_{1-x}Al_x)O_4$, x=0.1.

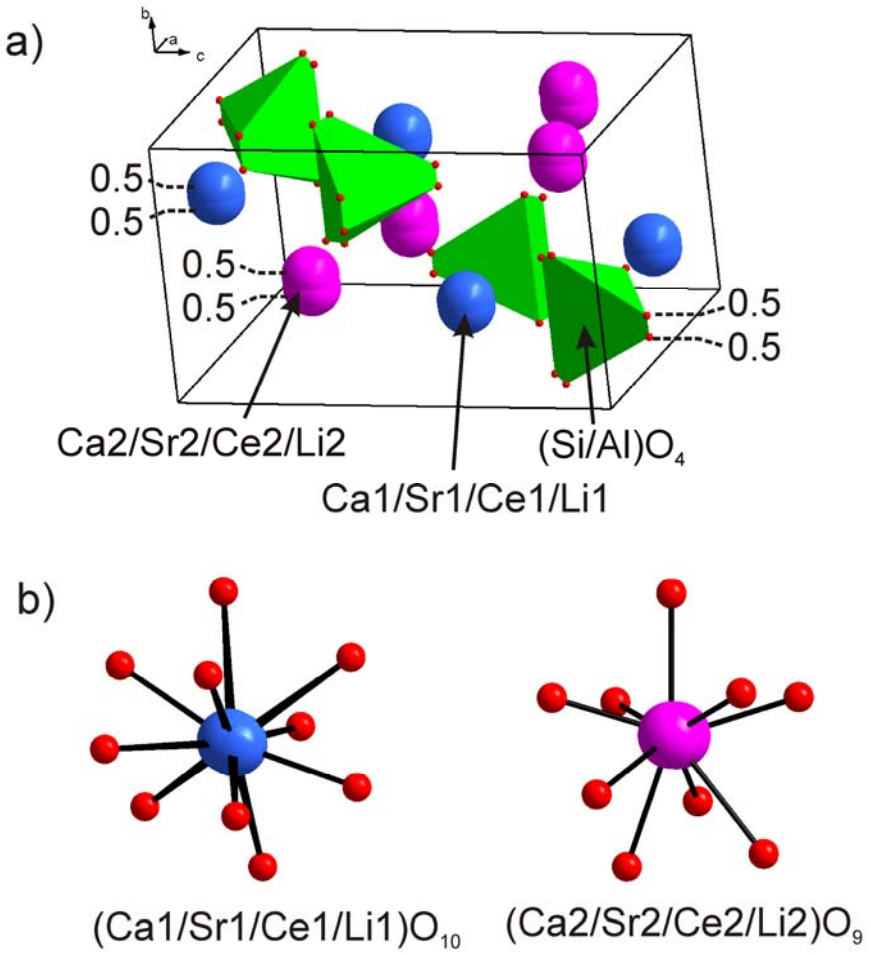

Figure 3 (a) Crystal structure of $(Ca_{0.95}Sr_{0.95}Ce_{0.05}Li_{0.05})(Si_{1-x}Al_x)O_4$; (b) coordination of Ca1/Sr1 and Ca2/Sr2 ions doped by Ce^{3+} and Li^+.

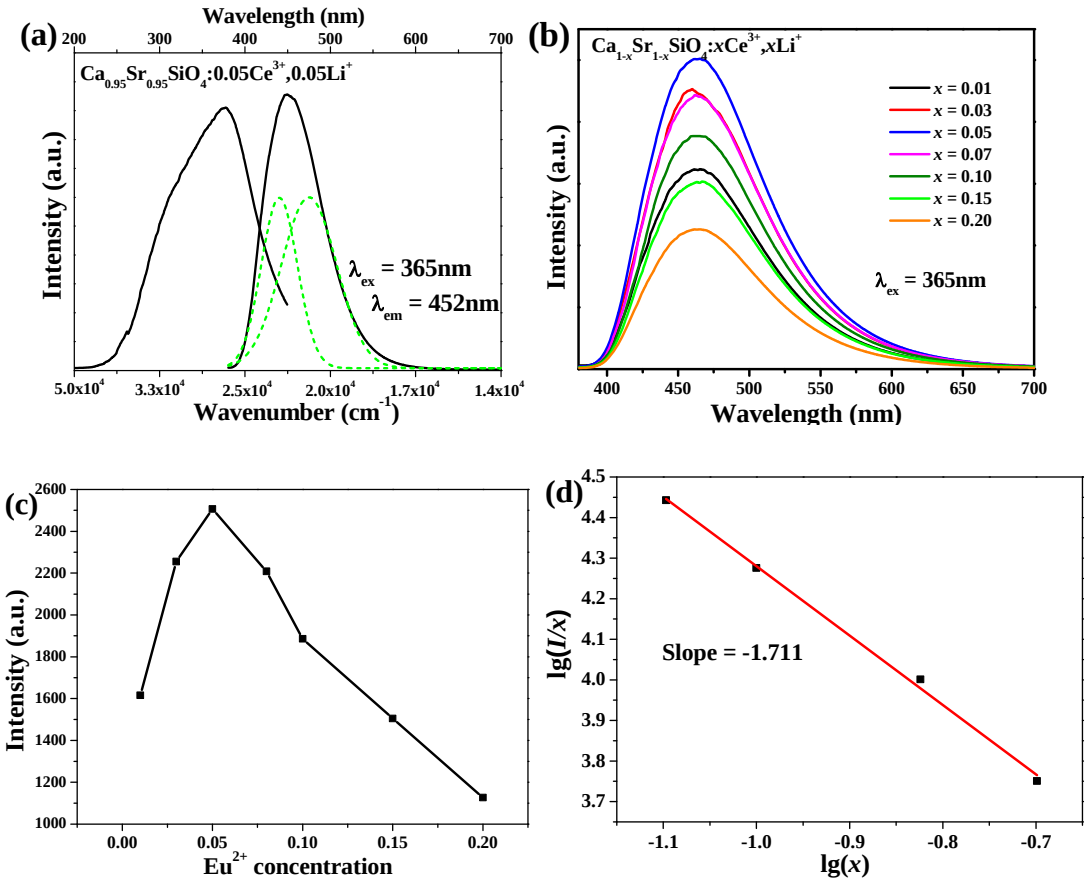

Figure 4 (a) PLE and PL spectra of $Ca_{0.95}Sr_{0.95}SiO_4:0.05Ce^{3+},0.05Li^+$ and the Gaussian fitting of the PL spectrum, (b) PL spectra of $Ca_{1-x}Sr_{1-x}SiO_4:xCe^{3+},xLi^+$ (x = 0.01, 0.03, 0.05, 0.08 and 0.10). (c) The PL intensity of the plot of $Ca_{1-2x}SrSiO_4:xCe^{3+},xLi^+$ as a function of Ce^{3+} content. (d) The relationships of lg(x) versus lg(I/x).

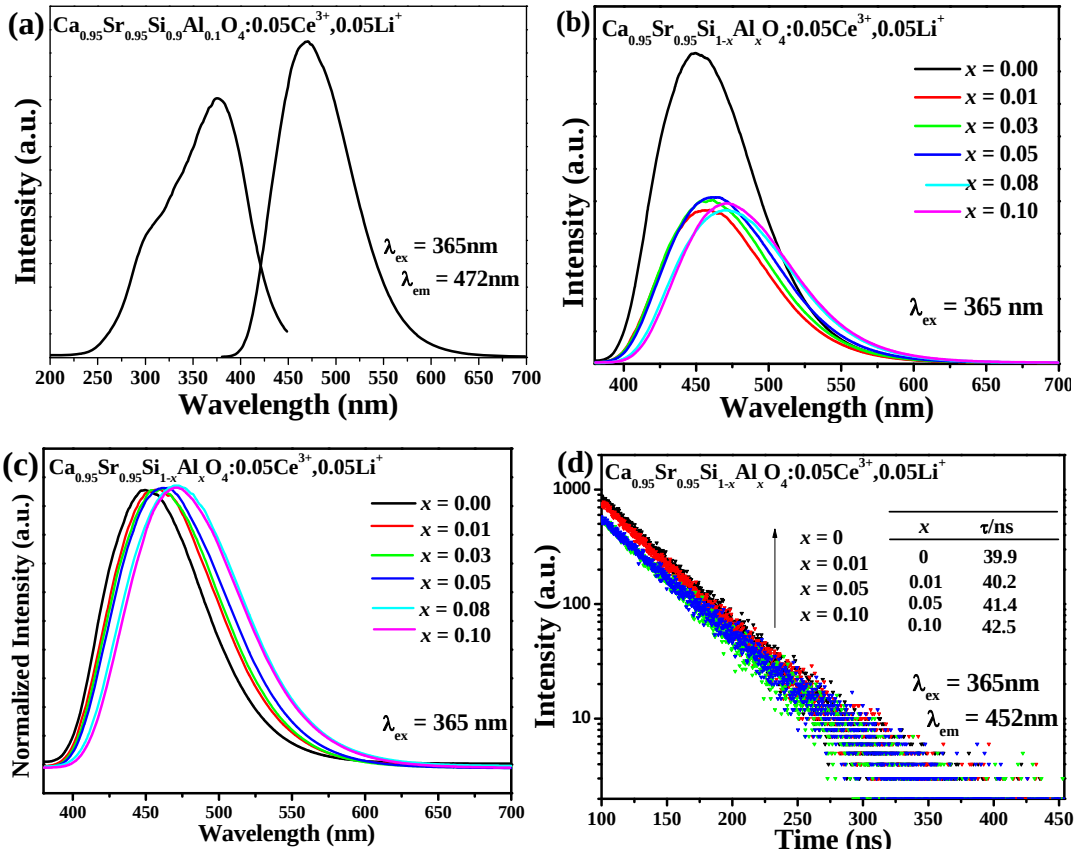

Figure 5 (a) PLE and PL spectra of $Ca_{0.95}Sr_{0.95}Si_{0.9}Al_{0.1}O_4$:0.05$Ce^{3+}$,0.05$Li^+$, (b) PL spectra of $Ca_{0.95}Sr_{0.95}Si_{1-x}Al_xO_4$:$x$$Ce^{3+}$,$x$$Li^+$ (x = 0, 0.01, 0.03, 0.05, 0.08 and 0.10), (c) the normalized PL spectra. (d) Decay curves of Ce^{3+} emission in $Ca_{0.95}Sr_{0.95}Si_{1-x}Al_xO_4$:0.05$Ce^{3+}$,0.05$Li^+$ phosphors under excitation at 365 nm, monitored at 452 nm.

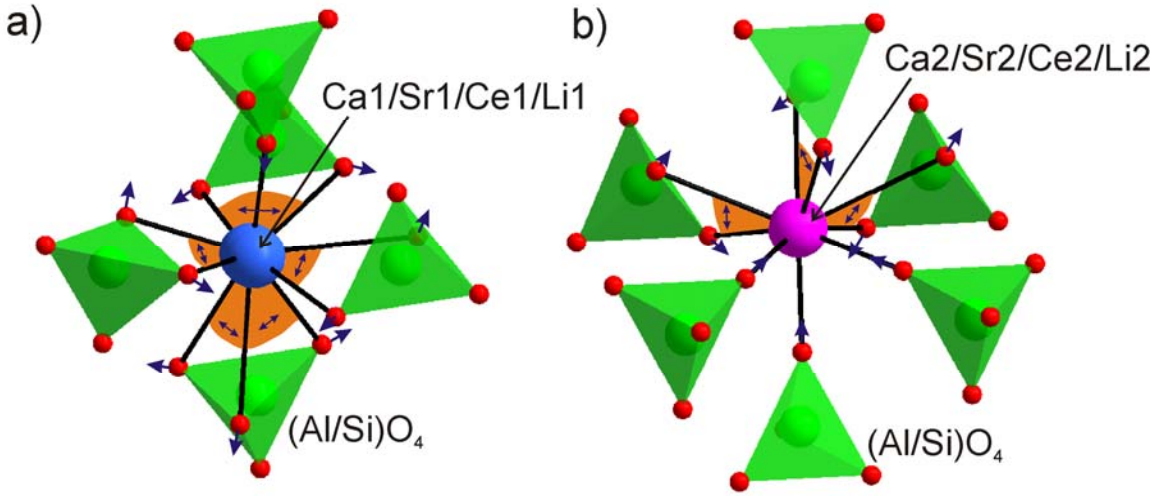

Figure 6 Mechanism of distortion polyhedra: (a) $(Ca1/Sr1/Ce1/Li1)O_{10}$; (b) $(Ca2/Sr2/Ce2/Li2)O_9$ with increasing of $(Al/Si)O_4$ tetrahedra size. Blue arrows show structure changes with increasing Al concentration, *x*. Angles O–(Ca/Sr/Ce/Li)–O, which increase their values with *x*, are marked by orange sectors.

Effect of Al/Si Substitution on the Structure and Luminescence Properties of $CaSrSiO_4:Ce^{3+}$ Phosphor: Analysis based on the Polyhedral Distortion†

Shihai Miao[1], Zhiguo Xia[1,2,*], Maxim S. Molokeev[3,4], Mingyue Chen[2], Jie Zhang[1], Quanlin Liu[2]

Polyhedra distortion originated from the variation of $[(Si,Al)O_4]$ induced the red-shift of the Ce^{3+} emission in $CaSrSi_{1-x}Al_xO_4:Ce^{3+},Li^+$ phosphor.